AIAA 93-1318
Hypersonic Flutter of a Curved Shallow Panel with Aerodynamic Heating

T. Bein, P. Friedmann, X. Zhong, and I. Nydick
Mechanical, Aerospace and
Nuclear Engineering Department
University of California
Los Angeles, CA

34th
AIAA/ASME/ASCE/AHS/ASC
Structures, Structural Dynamics and Materials Conference
AIAA/ASME
Adaptive Structures Forum
April 19-22, 1993 / La Jolla, CA

HYPERSONIC FLUTTER OF A CURVED SHALLOW PANEL WITH AERODYNAMIC HEATING

T. Bein†, P. Friedmann‡, X. Zhong* and I. Nydick**
Mechanical, Aerospace and Nuclear Engineering Department
University of California
Los Angeles, California 90024-1597

Abstract

The general equations describing the nonlinear fluttering oscillations of shallow, curved, heated orthotropic panels have been derived. The formulation takes into account the location of the panel on the surface of a generic hypersonic vehicle, when calculating the aerodynamic loads. It is also shown that third order piston theory produces unsteady aerodynamic loading which is in close agreement with that based upon direct solution of the Euler equations. Results, for simply supported panels, are obtained using Galerkin's method combined with direct numerical integration in time to compute stable limit cycle amplitudes. These results illustrate the sensitivity of the aeroelastic behavior to the unsteady aerodynamic assumptions, temperature, orthotropicity and flow orientation.

Nomenclature

a	plate length
a_∞	speed of sound
A	prescribed amplitude of panel motion
b	plate width
c_p	pressure coefficient
D_x,D_y	plate stiffness in the x and y directions, respectively
e	energy per unit volume
E_x,E_y	modulus of elasticity in the x and y directions, respectively
$\{f_{NL}\}$	right hand side of equations of motion, including all nonlinear terms
F	Airy stress function
F_h,F_p	homogeneous and particular parts of F
$\bar{F}$	quantity used in Euler equations
G_{xy}	shear modulus
$\bar{G}$	quantity used in Euler equations
h	plate thickness
H	height or maximum thickness of vehicle
i,k,n,r	indices associated with mode shapes in x-direction
j,ℓ,m,s	indices associated with mode shapes in the y-direction
k	spring stiffness
K_f	nondimensional frequency
K	hypersonic similarity parameter
L	maximum length of vehicle
$L[\ ]$	differential operator, representing equation of motion
M	Mach number
M_x^T,M_y^T	thermal moment intensity resultants
N_x^T,N_y^T	thermal stress intensity resultants
N_ℓ,N_w	number of modes in x and y directions, respectively
p	pressure
Δp	$p - p_\infty$
q_A	aerodynamic loading on the panel
R	gas constant
R_c	representative radius of curvature for vehicle surface

† Visiting Scholar, Technical University Aachen, Aachen, Germany
‡ Professor, Fellow AIAA, Member AHS, ASME
* Assistant Professor, Member AIAA
**Graduate Assistant

t time
T temperature distribution on the plate
T_{cr} critical temperature for panel buckling
T_{nm} generalized coordinate of panel motion
u,v velocity components
$\bar{U}$ quantity used in the Euler equations
V velocity
w panel deflection
x,y,z coordinates for panel
$\bar{x},\bar{y},\bar{z}$ coordinates for vehicle surface
$\{Y\}$ state variable vector
Z initial curvature of panel
Z_{nm} Fourier coefficients of initial curvature

Greek Symbols

α_x,α_y coefficient of thermal expansion in x and y directions
α flow orientation angle with respect to x-axis
β $\sqrt{M^2-1}$
γ ratio of specific heats
ε structural damping
$\varepsilon_{xx},\varepsilon_{yy},\varepsilon_{xy}$ strain components
θ_b flow deflection angle, semiangle representative of body surface
$\kappa_{xx},\kappa_{yy},\kappa_{xy}$ curvatures
λ nondimensional dynamic pressure parameter
λ_{cr} critical value of λ at which linear system becomes unstable
μ $31-\nu_{xy}\nu_{yx}$
$\bar{\nu}$ panel mass ratio
$\nu_{xy}\nu_{yx}$ Poisson's ratio in x and y direction
ξ,η non-dimensional coordinates in the x and y directions
ρ free stream air density
ρ_o panel density
τ non-dimensional time
ω panel frequency

Special Symbols

$(\dot{})$ derivative with respect to time
$()_\infty$ value at undisturbed flow
$()_p$ value on the surface of piston
$()_1$ value behind the shock
$()^0$ value on the middle surface
$(\bar{})$ nondimensional quantities

1. Introduction and Problem Statement

Renewed interest in the design of hypersonic vehicles motivated by the National Aerospace Plane (NASP) has generated a substantial number of new studies dealing with the aeroelastic, aerothermoelastic, and aeroservoelastic behavior of a generic vehicle resembling a potential NASP configuration[1-3]. Due to the preliminary nature of the studies, they have been based on a number of simplifying assumptions, the most restrictive of these being the use of linear piston theory for calculating the aerodynamic loads, and neglect of the details of the heat transfer process between the flow and the vehicle.

Other studies have restricted themselves to the treatment of a structural element representing the skin of a NASP-type vehicle, and conducted a variety of hypersonic panel flutter studies for isotropic and composite panels of hypersonic speeds[6-10]. Again, the unsteady loads in these analyses were based upon piston theory, and it is implicitly assumed that a panel in hypersonic flow is, indeed, representative of the conditions encountered by a structural element located on the surface of a generic NASP vehicle. Another interesting approach, pursued in Ref. 11, was based on obtaining the aerodynamic loads by assuming free-molecule flow. This condition corresponds to what may be encountered on the leeward portion of the hypersonic vehicle travelling at high altitudes. It was shown[11] that such aerodynamic shear effects can have some importance on the nonlinear aeroelastic behavior.

While the isolated panel flutter problem in hypersonic flow is significant, the problem becomes more complicated when some additional considerations, representative of the actual conditions present on the surface of a generic hypersonic vehicle, are taken into account. A generic hypersonic vehicle is shown in Fig. 1. It will generally consist of a curved surface, thus the panel will have initial curvature, and its location on the surface of the vehicle may have considerable influence on the aerodynamic loads to which the panel is exposed.

The temperature distribution over the vehicle, and the heat transfer between the skin and the surrounding fluid could also influence the aeroelastic behavior. The direction of the flow will rarely coincide with the edges of the panel. Furthermore, the difficulties associated with the wind tunnel testing of hypersonic vehicles imply that, for a better representation of the unsteady aerodynamic loads acting on the surface of such a vehicle, computational fluid dynamics (CFD) will have to be used. Therefore, it is interesting to examine to what extent the unsteady aerodynamic loads obtained from CFD methods, differ from the approximate loads obtained from piston theory.

The present paper is an exploratory study in which some of the questions raised above are studied. In this study we take advantage of the large number of papers which have been generated on panel flutter from the late 50's to the mid 70's. Without attempting to present a complete review of previous work on panel flutter, a few relevant previous studies are briefly mentioned below.

Most early work on panel flutter was restricted to supersonic speeds ($1.5 < M < 3.0$). A complete discussion of the fundamental aspects of panel flutter was given by Dugundji[12] using a linear, isotropic plate theory and a linear aerodynamic theory. At the same time the effect of temperature distribution on panel flutter was also considered[13]. It was also recognized that geometrical nonlinearities, due to moderate panel deflections, can play an important role in panel flutter. This led to a number of studies which emphasized the geometrically nonlinear aspects of panel flutter using a moderate deflection type of plate theory such as von Karman plate theory combined with first order piston theory for generating the unsteady aerodynamic loads[14-19]. These studies showed that when geometrical nonlinearities are included, the linear stability boundary can be exceeded and the panel develops, in most cases, stable limit cycle oscillations with amplitudes having an order of magnitude equal to the thickness of the panel. A comprehensive review of panel flutter problems is available in a monograph written by Dowell[17].

The objectives of this paper are: (a) to formulate the moderate deflection orthotropic, curved, panel flutter problem in hypersonic flow; (b) determine the accuracy of the unsteady aerodynamic loading based on piston theory by comparing it to results obtained from solution of the Euler equations for the hypersonic Mach numbers considered; and (c) to determine the influence of temperature, orthotropicity, panel location, orientation, and curvature on the aeroelastic behavior.

The numerical results presented illustrate panel behavior by presenting the sensitivity of the limit cycle amplitudes, to the parameters listed above.

2. Formulation of the Problem

The geometry of the problem is depicted in Fig. 2. It is assumed that the panel is built of an orthotropic material characterized by four elastic constants E_x, E_y, ν_{xy} and ν_{yx}, and thermal expansion coefficients α_x, α_y, where the thermal expansion coefficient in the xy direction is assumed to be zero for the orthotropic case. The panel is loaded by transverse loading and is subject to a temperature change from the initial stress free state.

Nonlinear panel flutter studies were frequently based on moderate deflection nonlinear plate theories such as the von Karman plate theory. In this study a further refinement is introduced by adopting Marguerre plate theory[20-21] which can also account for the initial curvatures of the panel. Marguerre theory was initially presented for the isotropic case in Ref. 20, and summaries of the theory can also be found in Ref. 21. The initial curvature of the panel, which is assumed to be shallow is defined by $Z(x,y)$. The other aspects of this theory are similar to von Karman type of thin plate theory. The extension of the theory from the isotropic case of the orthotropic case, carried out here, is fairly straightforward and the details of the derivation will be omitted for the sake of brevity.

The middle surface strains and curvatures for this theory are given by

$$\varepsilon_{xx}^0 = \frac{\partial u^0}{\partial x} + \frac{1}{2}\left(\frac{\partial w}{\partial x}\right)^2 + \frac{\partial Z}{\partial x}\frac{\partial w}{\partial x}$$

$$\varepsilon_{yy}^0 = \frac{\partial v^0}{\partial y} + \frac{1}{2}\left(\frac{\partial w}{\partial y}\right)^2 + \frac{\partial Z}{\partial y}\frac{\partial w}{\partial y} \qquad (2)$$

$$\varepsilon_{xy}^0 = \frac{\partial v^0}{\partial x} + \frac{\partial u^0}{\partial y} + \frac{\partial w}{\partial x}\frac{\partial w}{\partial y} + \frac{\partial Z}{\partial x}\frac{\partial w}{\partial y} + \frac{\partial Z}{\partial y}\frac{\partial w}{\partial x}$$

and

$$\kappa_x = -\frac{\partial^2 w}{\partial x^2}$$

$$\kappa_y = -\frac{\partial^2 w}{\partial y^2} \qquad (3)$$

$$\kappa_{xy} = -2\frac{\partial^2 w}{\partial x \partial y}$$

and the stress-strain relations are given by

$$\sigma_{xx} = \frac{E_x}{\mu}\varepsilon_{xx} + \frac{\nu_{xy}}{\mu}E_y\varepsilon_{yy} - \frac{E_x}{\mu}\alpha_x T - \frac{\nu_{xy}}{\mu}E_y\alpha_y T$$

$$\sigma_{yy} = \frac{E_y}{\mu}\varepsilon_{yy} + \frac{\nu_{xy}}{\mu}E_y\varepsilon_{xx} - \frac{E_y}{\mu}\alpha_y T - \frac{\nu_{xy}}{\mu}E_y\alpha_x T \qquad (4)$$

$$\sigma_{xy} = G_{xy}\varepsilon_{xy}$$

With these assumptions the equations of motion for the orthotropic panel can be written in the following manner.

$$D_x\frac{\partial^4 w}{\partial x^4} + 2(D_x\nu_{yx} + D_{xy})\frac{\partial^4 w}{\partial x^2\partial y^2} + D_y\frac{\partial^4 w}{\partial y^4}$$

$$-\frac{\partial^2 F}{\partial y^2}\left(\frac{\partial^2 w}{\partial x^2} + \frac{\partial^2 Z}{\partial x^2}\right) - \frac{\partial^2 F}{\partial x^2}\left(\frac{\partial^2 w}{\partial y^2} + \frac{\partial^2 Z}{\partial y^2}\right) \qquad (5)$$

$$+2\frac{\partial^2 F}{\partial x\partial y}\left(\frac{\partial^2 w}{\partial x\partial y} + \frac{\partial^2 Z}{\partial x\partial y}\right) + \frac{\partial^2 M_x^T}{\partial x^2} + \frac{\partial^2 M_y^T}{\partial y^2}$$

$$= -\rho_0 h\frac{\partial^2 w}{\partial t^2} - \rho_0 h\varepsilon\frac{\partial w}{\partial t} + q_A(x,y,t)$$

where F in Eq. (4) is the Airy stress function, given by

$$\frac{1}{E_y h}\frac{\partial^4 F}{\partial x^4} - \frac{2}{h}\left(\frac{\nu_{xy}}{E_x} - \frac{1}{2G_{xy}}\right)\frac{\partial^4 F}{\partial x^2\partial y^2}$$

$$+\frac{1}{E_x h}\frac{\partial^4 F}{\partial y^4} + \frac{\partial^2 w}{\partial x^2}\frac{\partial^2 w}{\partial y^2} - \left(\frac{\partial^2 w}{\partial x\partial y}\right)^2$$

$$+\frac{\partial^2 Z}{\partial x^2}\frac{\partial^2 w}{\partial y^2} + \frac{\partial^2 Z}{\partial y^2}\frac{\partial^2 w}{\partial x^2} - 2\frac{\partial^2 Z}{\partial x\partial y}\frac{\partial^2 w}{\partial x\partial y} \qquad (6)$$

$$= -\frac{1}{E_x h}\frac{\partial^2 N_x^T}{\partial y^2} - \frac{1}{E_y h}\frac{\partial^2 N_y^T}{\partial x^2}$$

$$+\frac{\nu_{xy}}{E_x h}\left(\frac{\partial^2 N_y^T}{\partial y^2} + \frac{\partial^2 N_x^T}{\partial x^2}\right)$$

where the following definitions have been used.

$$D_x = \frac{E_x h^3}{12\mu};\quad D_y = \frac{E_y h^3}{12\mu};\quad D_{xy} = \frac{G_{xy}h^3}{6};$$

$$\nu_{xy}E_y = \nu_{yx}E_x \quad \text{and} \quad \mu = 1 - \nu_{xy}\nu_{yx}$$

The thermal stress and moment intensity resultants are given by

$$N_x^T = \int_{-\frac{h}{2}}^{\frac{h}{2}}\left(\frac{E_x}{\mu}\alpha_x + \nu_{xy}\frac{E_y}{\mu}\alpha_y\right)T\,dz \qquad (7a)$$

$$N_y^T = \int_{-\frac{h}{2}}^{\frac{h}{2}}\left(\frac{E_y}{\mu}\alpha_y + \nu_{xy}\frac{E_y}{\mu}\alpha_x\right)T\,dz \qquad (7b)$$

$$M_x^T = \int_{-\frac{h}{2}}^{\frac{h}{2}}\left(\frac{E_x}{\mu}\alpha_x + \nu_{xy}\frac{E_y}{\mu}\alpha_y\right)Tz\,dz \qquad (8)$$

$$M_y^T = \int_{-\frac{h}{2}}^{\frac{h}{2}}\left(\frac{E_y}{\mu}\alpha_y + \nu_{xy}\frac{E_y}{\mu}\alpha_x\right)Tz\,dz \qquad (9)$$

The boundary conditions associated with this problem are those corresponding to a simply supported plate along its four edges.

It should also be noted that the Marguerre equations for a shallow curved panel are appropriate when the criterion for shallowness is defined as $(h/R_c) < 0.02$, where R_c is a representative radius of curvature.

2.1 Aerodynamic Loads

Hypersonic flow, which usually implies Mach numbers above 5 is substantially different from subsonic or supersonic flow. Depending on the precise conditions, high temperature effects, viscosity and even a chemically reacting boundary layer can be important. In fact, for many steady or unsteady hypersonic flow problems, analytical solutions are not available in the literature[22].

The exploratory nature of this study justifies the assumption of inviscid, continuum hypersonic flow over a slender body. In this case the shock wave lies close to the body and the shock angle is small, in such cases the hypersonic flow can be approximated by the hypersonic equivalence principle (Ref. 22, pp. 118). Combining it with strip theory for slender bodies with elliptical cross-sections allows one to approximate the pressure on the surface of the body (or panel) by the pressure distribution on an unsteady, one dimensional piston given by

$$\frac{p}{p_1} = \left(1 + \frac{\gamma - 1}{2}\frac{v_p}{a_1}\right)^{2\gamma/\gamma - 1} \tag{10}$$

where v_p is the velocity of the piston, while p_1 and a_1 are the pressure and sound velocity at the beginning of motion[23].

Equation (10) is equivalent to piston theory[4,5], except that in the case of hypersonic flow over a slender body, p_1 and a_1 are the values behind the shock. These values can be evaluated by using oblique shock relations, which utilize the hypersonic similarity parameter, K, defined as[22] $K = M_\infty \theta_b$, where θ_b is a flow deflection angle, which can also be related to the semi-angle of the body. The oblique shock relations can be written as

$$\frac{p_1}{p_\infty} = 1 + \frac{\gamma(\gamma+1)}{4}K^2 + \gamma K^2\sqrt{\left(\frac{\gamma+1}{4}\right)^2 + \frac{1}{K^2}} \tag{11}$$

$$\frac{\rho_1}{\rho_\infty} = \frac{(\gamma+1)K^2 S_p + \gamma + 1}{(\gamma-1)K^2 S_p + \gamma + 1} \tag{12}$$

$$S_p = \left[\frac{(\gamma+1)^2}{8} + \frac{\gamma+1}{2}\sqrt{\left(\frac{\gamma+1}{4}\right)^2 + \frac{1}{K^2}}\right]$$

where

$$\frac{a_1}{a_\infty} = \sqrt{\frac{p_1}{p_\infty}\frac{\rho_\infty}{\rho_1}} \tag{13}$$

The velocity, v_p is a superposition of the velocity due to the changing body shape and the velocity due to the motion of the panel.

$$v_p = V_\infty\left(\frac{\partial Z}{\partial x} + \frac{\partial w}{\partial x}\right) + \frac{\partial w}{\partial t} = a_\infty M_\infty\left(\frac{\partial Z}{\partial x} + \frac{\partial w}{\partial x} + \frac{1}{V_\infty}\frac{\partial w}{\partial t}\right) \tag{14}$$

The velocity of the piston is limited, namely v_p can not exceed the speed of sound.

Using Eqs. (10) and (14) the pressure distribution can be expanded using the binomial theorem. It is common practice in the process to retain terms up to the third order, which implies a nonlinear piston theory. It is convenient to rewrite Eq. (10) as

$$\frac{p}{p_\infty} = \frac{p_1}{p_\infty}\left[1 + \gamma\frac{v_p}{a_1} + \gamma\frac{(\gamma+1)}{4}\left(\frac{v_p}{a_1}\right)^2 + \gamma\frac{(\gamma+1)}{12}\left(\frac{v^p}{a_1}\right)^3\right] \tag{15}$$

2.2 Temperature Distribution

The aerodynamic model used in this study is based on the assumption that there is no interaction between the flow and the panel temperature and the vehicle is flying at constant speed. Furthermore the use of a thin plate theory implies that it is reasonable to assume a uniform temperature distribution through the thickness of the plate. While in the formulation of the problem provision for introducing a general temperature distribution $T(x,y)$ exists, the actual results are computed for a uniform temperature distribution. For an isotropic plate, simply supported and uniformly heated (i.e. loaded in both directions) the critical temperature, which produces buckling is given by[24]

$$T_{cr} = \left(\frac{h}{a}\right)^2 \frac{\pi^2}{6\alpha(1+\nu)} \qquad (16)$$

2.3 Mathematical Representation of the Vehicle Surface

To study in a convenient manner the influence of panel location, on the surface of the vehicle, on its flutter characteristics a mathematical representation of the lifting body associated with a generic hypersonic vehicle is needed. An analytical expression which approximates such a configuration is a hyperboloid of two sheets, described by

$$\left(\frac{\bar{x}+c_1}{c_1^2}\right)^2 - \frac{\bar{y}^2}{c_2^2} - \frac{\bar{z}^2}{c_3^2} = 1 \qquad (x > 0) \qquad (17)$$

Equation (16) represents a hyperboloid shifted on the x-axis such that the vertex of the right surface is located at the origin. The parameters c_1, c_2, c_3 are selected so as to resemble the dimensions of the NASP (considered as a generic hypersonic vehicle)

$$\frac{\text{width}}{\text{length}} = \frac{1}{4} \qquad \frac{\text{height}}{\text{width}} = \frac{1}{3}$$

which yields

$$c_1 = 0.5L\bar{\gamma}_c; \quad c_2 = 0.5L\gamma_c\bar{\gamma}_c; \quad c_3 = L\gamma_c\bar{\gamma}_c/6$$

where $\bar{\gamma}_c = (1/64\,\gamma_c^2 - 1)$

$$\gamma_c = \frac{c_2}{c_1} \quad \text{and} \quad 0 < \gamma_c < 0.125$$

where γ_c may be adjusted to change the curvature of the surface. This surface satisfies the shallowness conditions, stated earlier, at most locations on the surface of the vehicle except the nose region.

Using the equation of the surface, Eq. (17), a coordinate transformation can be obtained which relates the global body coordinates, $\bar{x}$, $\bar{y}$, and $\bar{z}$, to the components of a position vector (r_x, r_y, r_z) which identifies the location of the panel corner, and the x, y local coordinates of the panel. Using these relations the equation of the shallow curved initially undeformed shape of the panel can be represented by

$$Z(x,y) = \frac{1}{2\lambda_1}\left[-\lambda_2 + \sqrt{\lambda_2^2 - 4\lambda_1\lambda_2}\right] \qquad (18)$$

where the quantities, λ_1, λ_2, λ_3 are complicated functions of $\bar{x}$, $\bar{y}$, $\bar{z}$, c_1, c_2, c_3 and r_x, r_y, and r_z. For the sake of brevity, these fairly long expressions are not given here.

In the actual equations of motion the initial shape of the curved panel is represented by

$$Z(x,y) = \sum_{n=1}^{N}\sum_{m=1}^{M} Z_{nm}\sin\left(\frac{n\pi x}{a}\right)\sin\left(\frac{m\pi y}{b}\right) \qquad (19)$$

where the Fourier coefficients are given by

$$Z_{nm} = \int_0^a\int_0^b Z(x,y)\sin\left(\frac{n\pi x}{a}\right)\sin\left(\frac{m\pi y}{b}\right)dxdy \qquad (20)$$

which is consistent with the boundary conditions of a simply supported panel.

3. Method of Solution

The equations of motion are solved by using Galerkin's method to eliminate the spatial dependence in the problem, and subsequently, the resulting ordinary

differential equation are integrated directly in the time domain[18].

The approximate solution is represented by

$$w(x,y,t) = \sum_{n=1}^{N}\sum_{m=1}^{N} T_{nm}\sin\frac{n\pi x}{a}\sin\frac{m\pi y}{b} \qquad (21)$$

which satisfies the boundary conditions of a simply supported panel.

The solution consists of two parts, finding a solution for the Airy stress function $F(x,y)$ and then applying Galerkin's method to obtain a set of nonlinear ordinary differential equations.

The Airy stress function has to satisfy Eq. (6). The solution consists of a homogeneous part F_h and a particular part F_p. The homogeneous solution satisfies Eq. (6) when all the terms not related to F are deleted

$$\frac{1}{E_y h}\frac{\partial^4 F}{\partial x^4} - \frac{2}{h}\left(\frac{\nu_{xy}}{E_x} - \frac{1}{2G_{xy}}\right)\frac{\partial^4 F}{\partial x^2\partial y^2} + \frac{1}{E_x h}\frac{\partial^4 F}{\partial y^4} = 0 \qquad (22)$$

which is satisfied by assuming a solution in the form

$$F_h(x,y) = \frac{1}{2}(C_1x^2 + C_2y^2 + C_3xy) \qquad (23)$$

The coefficients C_1, C_2 and C_3 can be obtained by using the in-plane boundary conditions, which imply no shear and zero displacements at the boundaries[18].

After a considerable amount of algebra one obtains

$$C_1 = \frac{1}{8}\frac{E_x h}{\mu}\left(\frac{\pi}{a}\right)^2\left(\frac{E_y}{E_x}\right)^2\sum_n\sum_m\left[\nu_{xy}h^2 + \left(\frac{a}{b}\right)^2 m^2\right] \cdot T_{nm}(T_{mm} + 2Z_{nm}) - \frac{E_x h}{\mu}(\alpha_y + \nu_{xy}\alpha_x)\Delta T$$

$$C_2 = \frac{1}{8}\frac{E_x h}{\mu}\left(\frac{\pi}{a}\right)^2\sum_n\sum_m\left[n^2 + \nu_{xy}\left(\frac{a}{b}\right)^2 m^2\right] \cdot T_{nm}(T_{mm} + 2Z_{nm}) - \frac{E_y h}{\mu}(\alpha_x + \nu_{yx}\alpha_y)\Delta T$$

$$C_3 = 0 \qquad (24)$$

The mathematical details required for the particular solution are quite lengthy and will not be presented here. However, an outline of this solution can be found in Ref. 18.

Next, the solution for the stress function F and the assumed solution, Eq. (20) are substituted into the differential equation of motion, Eq. (5) and the aerodynamic loading term Eq. (15), this procedure leads to lengthy expressions due to the retention of the third order terms in the piston theory and presence of the temperature dependent loads. At this stage a number of nondimensional definitions are introduced to facilitate the treatment of these equations. The nondimensional quantities are listed below

$$\tau = \frac{t}{\bar{t}}; \quad \bar{t} = \sqrt{\frac{\rho_0 h a^4}{D_x}}; \quad \xi = \frac{x}{a};$$
$$\eta = \frac{y}{b}; \quad \bar{w} = \frac{w}{h};$$
$$\bar{T}_{nm} = \frac{T_{nm}}{h}; \quad \bar{Z}_{nm} = \frac{Z_{nm}}{h};$$
$$\lambda = \rho\frac{V^2 a^3}{D_x M_\infty}; \quad \bar{\nu} = \frac{\rho a}{\rho_0 h} \qquad (25)$$

Next Galerkin's method is applied on the resulting mathematical expressions. This procedure can be symbolically written as

$$\int_0^1\int_0^1 L[w]\sin\pi s\xi\sin\pi r\eta\, d\xi d\eta = 0 \qquad (26)$$
$$\text{for } s = 1, N_q \quad r = 1, N_w$$

where N_q and N_w represent the number of modes selected in the x and y direction respectively. Since the flow on the surface of the panel is lined up with the x-direction, the number of modes used in this direction is taken to be four, i.e., $N_q = 4$. Previous research indicated that six modes in the flow direction produce converged solutions, however four modes provide good accuracy for an exploratory study, such as conducted in this paper. To be able to account for panel orthotropicity two modes were used in the y direction, i.e., $N_w = 2$.

Thus, the structural dynamic problem is represented by a total of 8 modes.

Carrying out the detailed algebraic operations required for the implementation of Eq. (26) involve a large amount of algebra, and results in lengthy algebraic expressions, due to the retention of the higher order terms in the piston theory. These steps are not presented here due to their excessive length. However, it should be noted that a detailed description of the steps involved is available in Ref. 18.

The resulting equations are transformed into first order form, which can be written symbolically as

$$\{\dot{Y}\} = \{f_{NL}(\underset{\sim}{Y}, \lambda, \Delta T, t)\} \tag{27}$$

where

$$\underset{\sim}{Y} = \begin{Bmatrix} \underset{\sim}{\dot{T}}_{nm} \\ \underset{\sim}{T}_{nm} \end{Bmatrix}$$

Equations (27) represent a system of nonlinear ordinary differential equations which are solved by direct numerical integration. In this study an available computer program based on the Adams PECE formulas[25], was used.

4. Alternative Representation of the Aerodynamic Load

In the discussion of the unsteady aerodynamic load we pointed out that piston theory can be viewed only as an approximation for the unsteady aerodynamic load. Using an exact numerical solution to the Euler equations can be viewed as a potentially better approximation, and one might be tempted to base aeroelastic studies in hypersonic flow, on such a solution.

Fortunately, for the case of panel flutter, a relatively simple calculation can be carried out to resolve this question. One can pick a simple two dimensional problem, in which both the motion and the deformed shape of the panel are prescribed and given by

$$\frac{w(x,t)}{h} = \left(\frac{A}{h}\right)\sin\left(\frac{2\pi x}{a}\right)\sin\omega t \tag{28}$$

For this case Eq. (15) can be used to write a pressure coefficient in nondimensional form, given by

$$\begin{aligned}\bar{\Delta p} = {} & \frac{2\lambda}{\beta}\left(\frac{h}{a}\right)\left(W_{,\xi} + \sqrt{\frac{\bar{\nu}}{\lambda\beta}}\, W_{,\tau}\right) \\ & + \frac{\lambda(\gamma+1)}{2}\left(\frac{h}{a}\right)^2\left(W_{,\xi} + \sqrt{\frac{\bar{\nu}}{\lambda\beta}}\, W_{,\tau}\right)^2 \\ & + \frac{\lambda\beta(\gamma+1)}{6}\left(\frac{h}{a}\right)^3\left(W_{,\xi} + \sqrt{\frac{\bar{\nu}}{\lambda\beta}}\, W_{,\tau}\right)^3\end{aligned} \tag{29}$$

and

$$W(\xi,\tau) = \left(\frac{A}{h}\right)\sin(2\pi\xi)\sin(K_f\tau) \tag{30}$$

where the following nondimensional quantities have been used in Eqs. (29) and (30)

$$\begin{aligned} & W = \left(\frac{w}{h}\right);\quad \Delta p = p - p_\infty;\quad \beta = \sqrt{M^2 - 1} \\ & \bar{\nu} = \frac{\rho}{\rho_p}\frac{a}{h};\quad K_f = \omega\bar{t};\quad \bar{\Delta p} = \frac{2\Delta p a^3}{\beta D x}\end{aligned} \tag{31}$$

Combining Eqs. (29)-(31) one has

$$\begin{aligned} c_p = {} & \frac{2}{\beta}\left(\frac{h}{a}\right)\left[C_{A1}(\xi)\sin K_f\tau + c_{A2}(\xi)\cos K_f\tau\right] \\ & + \frac{\gamma+1}{2}\left(\frac{h}{a}\right)^2\left[c_{A1}(\xi)\sin K_f\tau + C_{A2}(\xi)\cos K_f\tau\right]^2 \\ & = \beta\frac{(\gamma+1)}{6}\left(\frac{h}{a}\right)^3\left[c_{A1}(\xi)\sin K_f\tau + c_{A2}(\xi)\cos K_f\tau\right]^3\end{aligned} \tag{32}$$

where

$$c_{A1} = \frac{A}{h}2\pi\cos 2\pi\xi$$

$$c_{A2} = \left(\frac{A}{h}\right)\sqrt{\frac{\bar{\nu}}{\lambda\beta}}\, K_f \sin 2\pi\xi$$

In addition to calculating the unsteady pressure coefficient from Eq. (32), the pressure coefficient was

also obtained from the direct numerical solution of the Euler equations as described next.

The two-dimensional unsteady Euler equations are solved in a 66×38 Cartesian grid which is fixed during the computations. In the Cartesian coordinates, the Euler equations can be written in the following conservation-law form:

$$\frac{\partial \bar{U}}{\partial t} + \frac{\partial \bar{F}}{\partial x} + \frac{\partial \bar{G}}{\partial y} = 0 \qquad (33)$$

where $\bar{U} = [\rho, \rho u, \rho v, e]_T$, and

$$\bar{F} = \begin{Bmatrix} \rho u \\ \rho u^2 + p \\ \rho uv \\ eu + pu \end{Bmatrix}, \quad \bar{G} = \begin{Bmatrix} \rho v \\ \rho uv \\ \rho v^2 + p \\ ev + pv \end{Bmatrix} \qquad (34)$$

In the equations above, ρ, u, v, p, T, and e denote density, velocity components in x and y directions, pressure, temperature, and total energy per unit volume ($e = p/(\gamma - 1) + \rho(u^2 + v^2)/2$) respectively. The gas is assumed to be perfect gas with $\gamma = 1.4$ and gas constant $R = 287.04\ Nm/kg°K$.

The numerical method used for solving the conservation equations are the essentially nonoscillatory (ENO) schemes[26]. The ENO schemes were originally developed for computing high-speed flows with shock waves with high order accurate nonoscillatory solutions. Compared with other high resolution upwind schemes which are usually not uniformly high order accurate, the ENO schemes can achieve nonoscillatory solutions with uniformly high order accuracy in space and in time. Therefore, the ENO schemes are particularly suitable for computing loads for dynamic cases such as the flutter problem where high frequency transient flow fields exist. The ENO schemes have been applied to compressible viscous flow in an previous paper[27] and the same computer code is used here to solve the Euler equations for the moving panel problem.

The main features of the numerical method used in the present computations are as follows. The conservation equations are solved by using the finite volume method with second order ENO schemes. The ENO reconstruction is based on two-dimensional primitive functions of the conservation variables and numerical flux vectors are computed by using the Roe approximate Riemann solver. The time stepping scheme is the explicit TVD Runge-Kutta scheme with the order of accuracy in time being consistent with the order of accuracy in space. The details of the numerical methods used in the code can be found in Ref. 26.

The boundary conditions for the flow variables in the supersonic free stream are specified to the given values; the boundary conditions in the outflow boundaries are computed by using linear extrapolation from the interior of the flow field. Since the amplitude of the oscillation of the panel is very small compared with the length of the panel (1:225), the computational boundary at lower surface is fixed at $y = 0$, instead of moving with the panel, and the velocity boundary conditions at the wall surface $y = 0$ are specified as:

$$v - u\left(\frac{\partial y}{\partial x}\right) = \frac{\partial y}{\partial t} \qquad (35)$$

where $y = y(x,t)$ is the prescribed oscillation of the panel surface. The present approximate boundary treatment on the wall surface is suitable only for small amplitude oscillation. In the case of large amplitude motion, the grids can no longer be fixed and have to move with the wall.

The computational results in this paper are obtained by an explicit second order accurate ENO scheme in both space and in time. A CFL number of 0.5 is used for the time accurate computations. The other parameters used in the computations are listed below.

Mach Number	$M_\infty = 10.05$
Temperature	$T_\infty = 223.16\,(K)$
Pressure	$p_\infty = 2641.6\,(N/m^2)$
Surface Function	$y = A \sin\frac{\pi n x}{L} \sin\omega t$
$A = 0.002\,m$	$n = 2$
$\omega = 1.206 \times 10^3\,rad/\text{sec}$	$L = 0.45\,m$

The panel properties which are also relevant to these calculations are also given below:

$E = 69 \times 10^9\ N/m^2$; $\nu = 0.33$ (material aluminum);

$h = 0.002\ m$; $a = 0.45\ m$; $\rho_\infty = 2.77 \times 10^3\ Kg/m^3$

$D = 51.62\ N.m$; $K_f = 80$; $\gamma = 1.4$; $\beta = 10$

$\bar{\nu} = 0.03351$; $\lambda = 659.42$

Figures 4 and 5 depict a comparison of the pressure coefficient, obtained from piston theory and from the solution of the Euler equations plotted as a function of the nondimensional time. Figure 4 depicts c_p as a function of time at $\xi = 0.40$ and Fig. 5 presents the same information at $\xi = 0.85$. It is clear from these figures that the principal difference is between first order and second order piston theory. The results of the second order and third order piston theory (which are very close) are also in close agreement with the result obtained from the solution of the Euler equations for this particular Mach number and prescribed panel motion.

These results indicate that a similar comparison with the results obtained from the solution of the Navier-Stokes equations for the same test case, would be a useful endeavor.

5. Results and Discussion

The results obtained in this study are usually presented in the form of stable limit cycle amplitudes evaluated for values of the dynamic pressure parameter $\lambda > \lambda_{cr}$; where λ_{cr} is the critical value at which the linear panel flutter problem becomes unstable. The parameters which have been used in the calculation are given in Table. 1. The structural damping, $\epsilon = 0$, for all the calculations performed.

A typical limit cycle is shown in Fig. 6. Careful numerical tests were done for selecting the correct stepsize $\Delta\tau$ at which converged limit cycles are obtained. All the results presented in this section were obtained for flat panels.

As indicated in the previous section, the primary difference in pressure coefficients between linear, or first order piston theory, and higher order theories is due to the second order terms. The results presented in Fig. 7 show the influence of various orders of piston theory on the stability boundary and limit cycle amplitudes of isotropic panels. All the calculations are carried out with four modes in the streamwise direction, and two modes in the direction perpendicular to the flow direction. The limit cycles are evaluated at $\xi = 0.75$ and $\eta = 0.50$; between five to six values of $\lambda > \lambda_{cr}$ are used to generate a typical limit cycle amplitude plot as a function of λ. It is evident from the figure that the differences in limit cycle amplitudes are similar to the differences in pressure coefficients when one increases the order of piston theory. Figure 8 illustrates the behavior of the orthotropic panel, which for this case, resembles closely its isotropic counterpart. All subsequent results presented in this section were calculated for piston theory with third order terms included.

The influence of aerodynamic heating is considered next. A uniform temperature is imposed on the panel. For the isotropic case it is assumed that the panel is made of aluminum, with $\alpha_x = 1.2 \times 10^{-5}$/°F. Figure 9 shows the limit cycle amplitudes for three uniform temperature distributions $T = 5$°F, $T = 10$°F, and $T = 15$°F, imposed on the panel. It is evident that aerodynamic heating reduces λ_{cr} significantly and it also increases the limit cycle amplitudes. For the particular combination of panel geometry, material and boundary conditions increasing the temperature by 5°F from the initial stress free state reduces the critical dynamic pressure by 20% and leads to substantial increases in limit cycle amplitudes.

The influence of the temperature on the orthotropic panel is depicted in Fig. 10. For this case it is assumed that the panel is a graphite/epoxy orthotropic plate[28], with $\alpha_y/\alpha_x = 0.001$ and $\alpha_x = 2.1 \times 10^{-5}$/°F. The effect is somewhat more pronounced, than in the isotropic case, because the reduction in stiffness of the heated orthotropic panel exceeds that present in the isotropic case. These results clearly indicate the importance of carrying out a combined aeroelastic and heat transfer analysis where the temperature (equilibrium or time varying) is accurately obtained from the solution of the heat transfer problem.

Preliminary calculations, for which results are not presented here, were also done to determine the effects of nonuniform temperature in the x and y direction, on panel flutter. It appears that the correct value of the temperature, when assumed to be uniform over the area of the plate, is more important that its precise distribution in the x and y directions.

The shape of the hypersonic lifting body, and a representative panel, are schematically illustrated in Fig. 3. For such a configuration, variation in the hypersonic similarity parameter can be significant. Three values of the hypersonic similarity parameter, discussed in the aerodynamic loads section were considered: $K = 1$; $K = 1.25$ and $K = 1.5$ which correspond to a vehicle flying at $M_\infty = 10$ and having semiangles (of inclination or flow deflection) corresponding to $\theta_b = 5.7°$; $\theta_b = 7.2°$ and $\theta_b = 8.6°$. The results are shown in Fig. 11. It is evident from the figure that this effect, associated with the presence of shock waves influences both λ_{cr} as well as the magnitude of the limit cycle amplitude.

Finally, it is important to note that another flow related effect, which can have an influence similar to the hypersonic similarity parameter, is the flow orientation (or direction) which was studied in detail, in the context of conventional panel flutter in Ref. 18. This effect is due to the fact that the x and y directions which represent the edges of the panel will not, in practical cases, coincide with the flow direction. In the current study it was assumed that the flow is in the x-direction. In general, however, the flow will have an orientation angle α relative to the x-direction. For this case, Eq. (14) will have to be modified

$$v_p = a_\infty M_\infty \left[\frac{1}{V_\infty}\frac{\partial w}{\partial t} + \left(\frac{\partial Z}{\partial x} + \frac{\partial w}{\partial x} \right) \cos\alpha + \left(\frac{\partial Z}{\partial y} + \frac{\partial w}{\partial y} \right) \sin\alpha \right] \tag{36}$$

which leads to coupling of the panel vibrations in the x and y directions[18]. Figure 12, taken from 18, shows the effect of nonlinearity on the dynamic pressure ratio $(\lambda)_\alpha/(\lambda)_{\alpha=0}$ for two different isotropic panels. For $a/b = 1.0$, no difference is evident between $(\lambda)_\alpha/(\lambda)_{\alpha=0}$ for $(w/h) = 0.80$ and $(\lambda_{cr})_\alpha/(\lambda_{cr})_{\alpha=0}$ on the scale of the figure. For $(a/b) = 2.0$ nonlinearity slightly increase the effect of flow direction on the dynamic pressure ratio. For $(a/b) = 0.50$ the effect is much more substantial, and it is due to a combination of nonlinearity and aerodynamic damping.

6. Concluding Remarks

In this paper Marguerre shallow curved plate theory has been extended to the orthotropic case and used to study the hypersonic nonlinear flutter of panels undergoing moderate deflections.

It was found that for high Mach numbers the unsteady solution of the Euler equations using computational fluid mechanics gives virtually identical pressure distributions to that obtained from nonlinear third order piston theory.

The difference in limit cycle amplitudes obtained with linear and third order piston theory is of the order of 5-7%. It was also found that aerodynamic heating has a strong influence both on the critical dynamic pressure parameter λ_{cr} as well as on the amplitudes of the panel limit cycles. This suggests that the heat transfer problem governing the panel temperature should be solved together with the aeroelastic problem. Orthotropic panel construction can be more sensitive to temperature effects.

The hypersonic similarity parameter, panel location on the surface of a hypersonic lifting body, and relative orientation between the flow direction and the edges of the panel are important parameters which can significantly influence the aeroelastic behavior of structural elements constituting the skin of a generic hypersonic vehicle.

Acknowledgment

This research was supported by NASA grant NCC 2-374 provided under the auspices of the UCLA/NASA Dryden Flight Systems Research Center. The useful comments of the grant monitor, Dr. K. Gupta, from Dryden, are gratefully acknowledged.

References

1. Spain, C., Soistmann, D., Parker, E., Gibbons, M., and Gilbert, M., "An Overview of Selected NASP Aeroelastic Studies at NASA Langley Research Center," AIAA Paper No. 90-5218, AIAA Second International Aerospace Planes Conference, October 28-31, 1990, Orlando, FL.
2. Heeg, J., Gilbert, M.G., and Pototzky, A., "Active Control of Aerothermoelastic Effects for a Conceptual Hypersonic Aircraft," NASA TM 102TI3, August 1990.
3. Gilbert, M.G., Heeg, J., Pototzky, A.S., Spain, C.V., Soitsmann, D.L., and Dunn, H.J., "The Application of Active Controls Technology to a Generic Hypersonic Aircraft Configuration," NASP Technical Memorandum 1097, May, 1990.
4. Ashley, H., Zartarian, G., "Piston Theory - A New Aerodynamic Tool for the Aeroelastician," *J. Aeronautical Sciences*, Vol. 23, No. 10, 1956, pp. 1109-1118.
5. Lighthill, M.J., "Oscillating Airfoils at High Mach Number," *J. Aeronautical Sciences*, Vol. 20, No. 6, 1953, pp. 420-406.
6. Mei, C. and Gray, C., "A Finite-Element Method for Large-Amplitude, Two-Dimensional Panel Flutter at Hypersonic Speeds," Proc. 30th AIAA/ASME/ASCE/AHS Structures, Structural Dynamics and Materials Conference, Mobile, AL, April 1989, AIAA Paper No. 89-1165, pp. 37-51.
7. Xue, D.Y. and Mei, C., "Finite Element Two-Dimensional Panel Flutter at High Supersonic Speeds and Elevated Temperature," Proc. 31st AIAA/ASME/ASCE/AHS Structures, Structural Dynamics and Materials Conference, 1990 AIAA Paper No. 90-0982, pp. 1464-1475.
8. Xue, D.Y. and Mei, C., "Finite Element Nonlinear Flutter and Fatigue Life of 2-D Panels with Temperature Effects," Proc. 32nd AIAA/ASME/ASCE/AHS Structures, Structural Dynamics and Materials Conference, Baltimore, MD, April 8-10, 1991, AIAA Paper No. 91-1170, pp. 1981-1991.
9. Abbas, J.F. and Ibrahim, R.A., "Nonlinear Flutter of Orthotropic Composite Panel Under Aerodynamic Heating," AIAA Dynamics Specialist Conference, Dallas, TX, April 16-17, 1992, AIAA Paper No. 92-2132, 424-535.
10. Gray, Jr., E.G. and Mei, C., "Large-Amplitude Finite Element Flutter Analysis of Composite Panels in Hypersonic Flow," Proc. 33rd AIAA/ASME/ASCE/AHS Structures, Structural Dynamics and Materials Conference, Dallas, TX April 16-17, 1992, AIAA Paper No. 92-2130, pp. 492-512.
11. Resende, H.B., "Nonlinear Panel Flutter in a Rarefied Atmosphere: Aerodynamic Shear Stress Effects," AIAA Paper No. 91-1172-CP, Proc. 32nd AIAA/ASME/ASCE/AHS/ACS Structures, Structural Dynamics and Materials Conference, Baltimore, MD, April 8-10, 1992, pp. 1992-2001.
12. Dungundji, J., "Theoretical Considerations of Panel Flutter at High Supersonic Mach Numbers," *AIAA Journal*, Vol. 4, No. 7, July 1966, pp. 1257-1266.
13. Schaeffer H.G. and Heard, W.L., "Flutter of a Flat Panel Subjected to a Nonlinear Temperature Distribution," *AIAA Journal*, Vol. 3, No. 10, October 1965, pp. 1918-1923.
14. Bolotin, V.V., *Nonconservative Problems of the Theory of Elastic Stability*, Pergamon Press, 1963, pp. 274-312.
15. Dowell, E.H., "Nonlinear Oscillations of a Flutter Plate," *AIAA Journal*, Vol. 4, No. 7, July 1966, pp. 1267-1275.
16. Dowell, E.H., "Nonlinear Oscillations of a Fluttering Plate, II" *AIAA Journal*, Vol. 5, No. 10, October 1967, pp. 1856-1862.
17. Dowell, E.H., *Aeroelasticity of Plates and Shells*, Noordhoff International Publishing, Hyden, The Netherlands, 1975.
18. Friedmann, P. and Hanin, M., "Supersonic Non Linear Flutter of Orthotropic or Isotropic Panels with 'Arbitrary' Flow Direction," *Israel Journal Technology*, Vol. 6, No. 1-2, 1968, pp. 46-57.
19. Kuo, C.-C. and Morino, L., "Perturbation and Harmonic Balance Methods for Nonlinear Panel Flutter," *AIAA Journal*, Vol. 10, No. 11, November 1972, pp. 1479-1484.
20. Marguerre, K., "Zur Theorie der Gekrummten Platte Grosser Formanderung," Proc. 5th International Congress on Applied Mechanics, 1938, pp. 93-101.
21. Chia, C.Y., *Nonlinear Analysis of Plates*, McGraw Hill, New York, 1980.
22. Anderson, A.H., *Hypersonic and High Temperature Gas Dynamics*, McGraw-Hill, New York, 1989.
23. Shapiro, A.H., *The Dynamics and Thermodynamics of Compressible Fluid Flow*, Vol. II, The Ronald Press, New York, 1954, pp. 940-952.
24. Brush, D.O. and Almroth, B.O., *Buckling of Bars, Plates, and Shells*, McGraw Hill, 1975, pp. 103-105.
25. Shampine, L.F. and Gordon, M.K., *Computer Solution of Ordinary Differential Equations*, W.H. Freeman and Company, San Francisco, 1975.
26. Harten, A., Engquist, B., Osher, S., and Chakravarthy, S., "Uniformly High Order Accurate Essentially Non-oscillatory Schemes, III," *Journal of Computational Physics*, Vol. 71, No. 2, August 1987.

27. Zhong, X., "Application of High-order Accurate Essentially Nonoscillatory Schemes to Two-dimensional Compressible Viscous Flows," AIAA Paper No. 93-0879, AIAA Aerospace Science Meeting, January 1993, Reno, Nevada.

Table 1: Data Used in the Calculations

	Isotropic	Orthotropic
a/b	1	1
a/h	100	100
E_y/E_x	1	20
ν_{yx}	0.3	0.3
ν_{yx}/ν_{xy}	1	20
$\rho_\infty/\rho\ a/h$	1	1
M_∞	10	10
modes	4×2	4×2
ξ	0.75	0.75
η	0.5	0.5

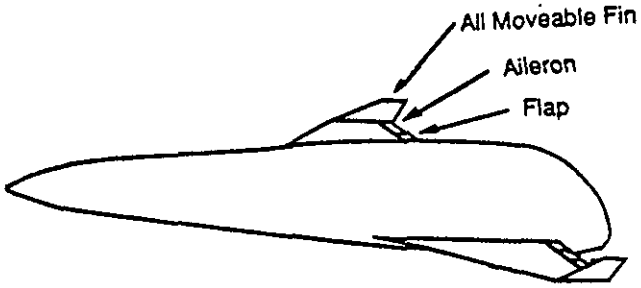

Figure 1: Schematic Representation of a Generic Hypersonic Vehicle.

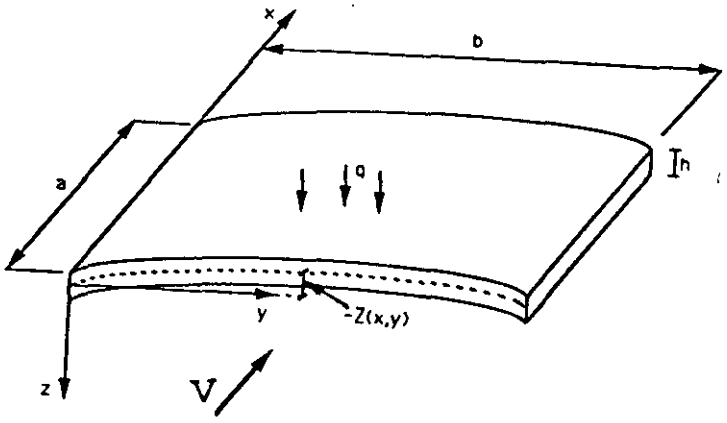

Figure 2: Definition of Panel Geometry.

28. Sun, C.T. and Chen, J.J, "Transient Thermal Stress Analysis in Graphite/Epoxy Composite Laminates," *Developments in Theoretical and Applied Mechanics*, Vol. 11, 1982, pp. 309-328.

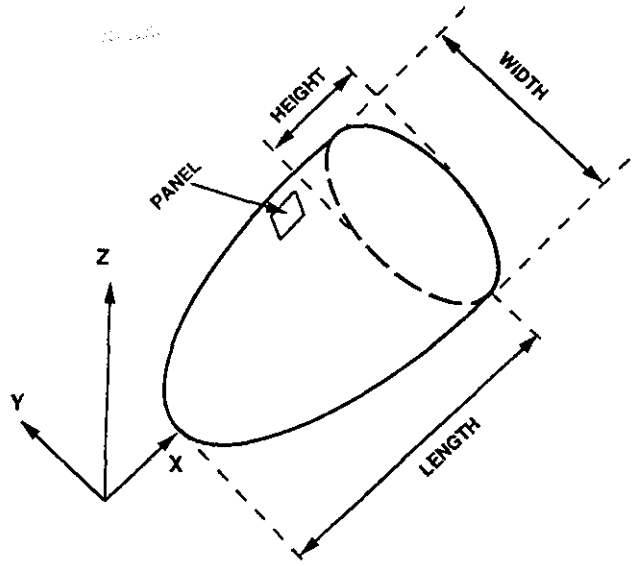

Figure 3: Schematic Representation of Hypersonic Vehicle Body.

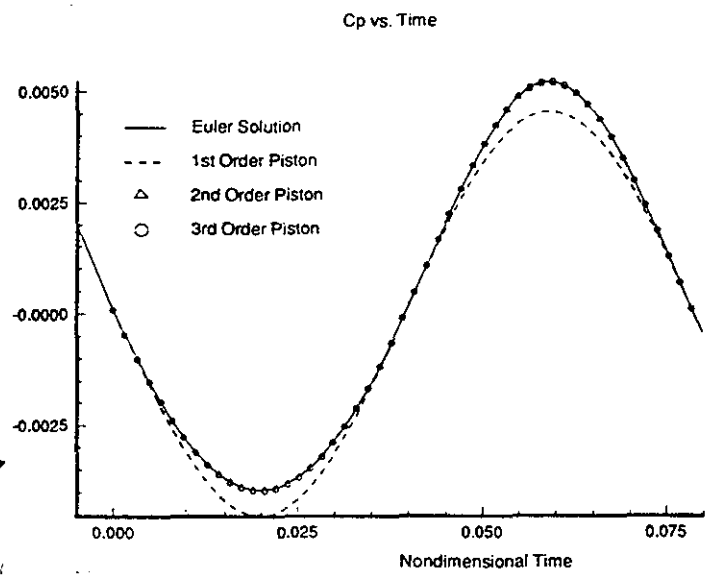

Figure 4: Pressure Coefficient vs. Time, Two-dimensional Panel, Comparison of Euler Solutions with Piston Theory; $\xi = 0.40$.

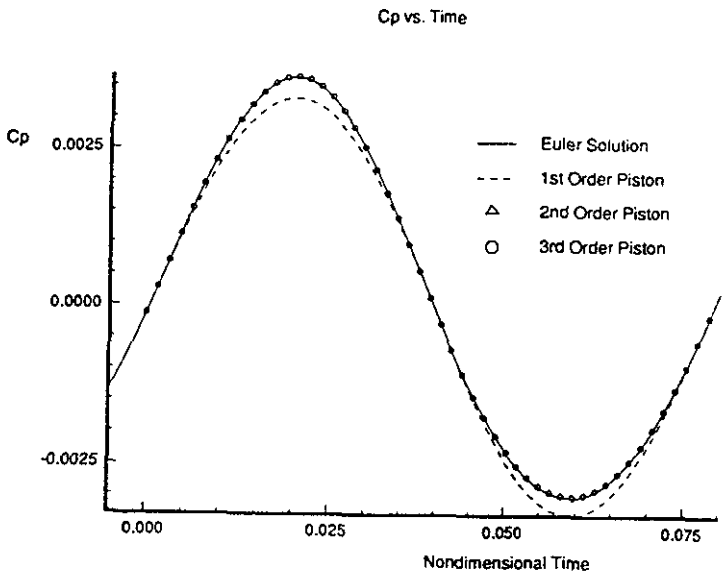

Figure 5: Pressure Coefficient vs. Time, Two-dimensional Panel, Comparison of Euler Solution with Piston Theory; $\xi = 0.85$.

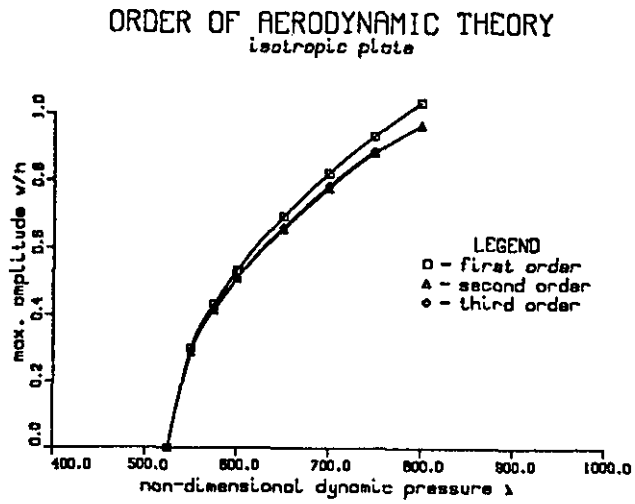

Figure 7: Influence of Various Orders of Piston Theory for Isotropic Panel.

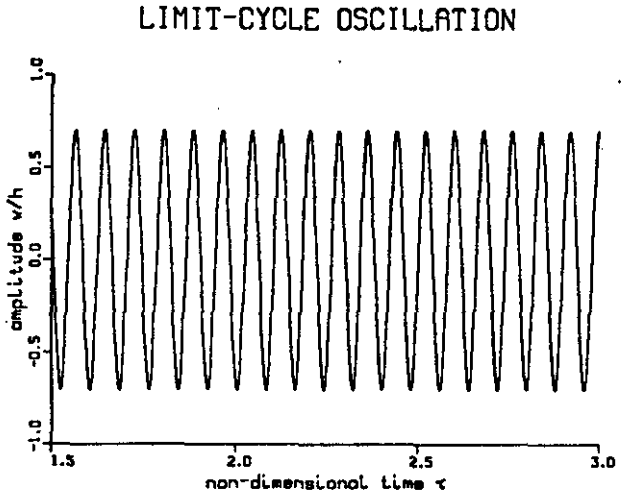

Figure 6: Typical Limit Cycle Oscillation ($\lambda = 650$).

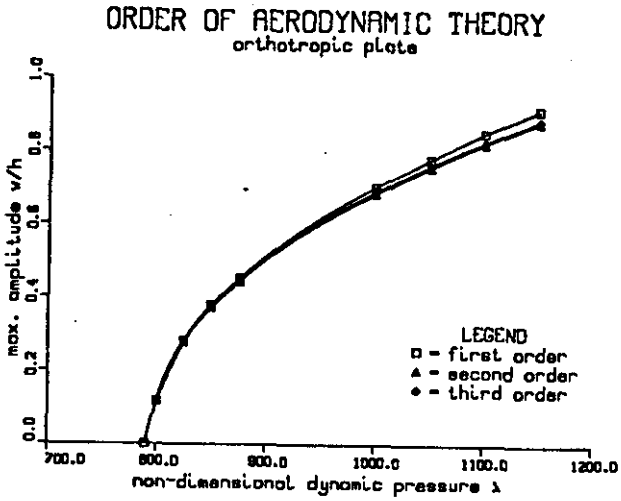

Figure 8: Influence of Various Order of Piston Theory for Orthotropic Panel.

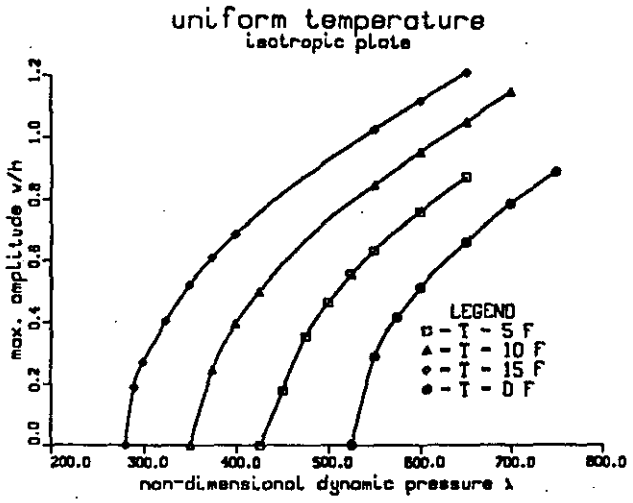

Figure 9: Influence of Uniform Temperature Distribution on Isotropic Panel.

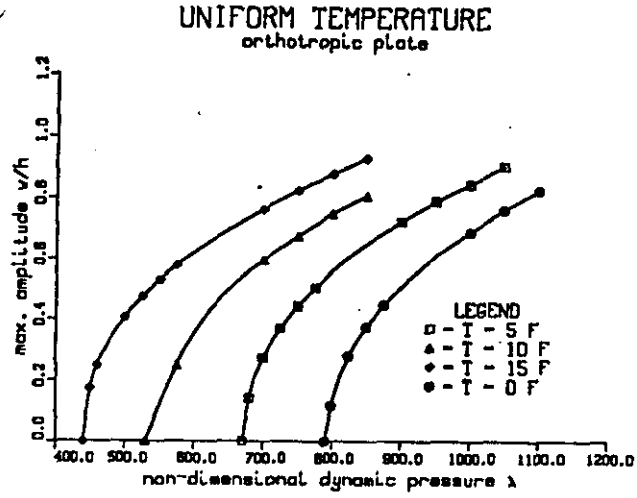

Figure 10: Influence of Uniform Temperature Distribution on Orthrotropic Panel.

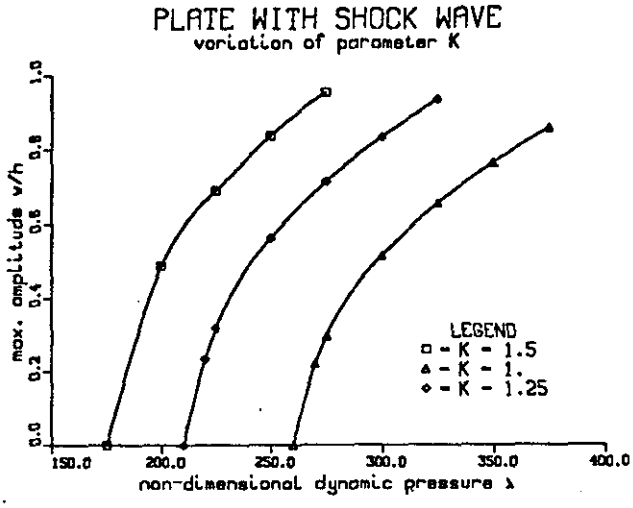

Figure 11: Influence of Hypersonic Similiarity Parameter, K, (shock wave) on stability of orthotropic panel.

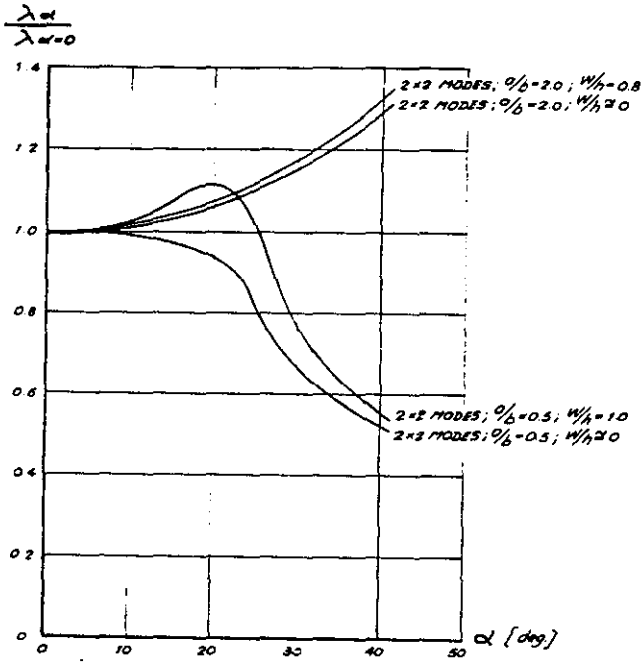

Figure 12: Effect of Flow Orientation on λ_{cr} and Limit Cycle Flutter Amplitude for Various Aspect Ratio Panels, from Ref. 18.